Harmonic Stability Assessment for Multi-Paralleled, Grid-Connected Inverters

Yoon, Changwoo; Wang, Xiongfei; Silva, Filipe Miguel Faria da; Bak, Claus Leth; Blaabjerg, Frede

Published in:
Proceedings of the IEEE International Power Electronics and Application Conference and Exposition (IEEE PEAC'14)

DOI (link to publication from Publisher):
10.1109/PEAC.2014.7038014

Publication date:
2014

Document Version
Early version, also known as pre-print

Harmonic Stability Assessment for Multi-Paralleled, Grid-Connected Inverters

Changwoo Yoon, Xiongfei Wang, Filipe Miguel Faria Da Silva, Claus Leth Bak and Frede Blaabjerg
Department of Energy Technology
Aalborg University
Aalborg, Denmark
cyo@et.aau.dk

Abstract—***This paper investigates the dynamic interactions of current controllers for multi-paralleled, grid-connected inverters. The consequent harmonics instability phenomena, which features with oscillations above the fundamental frequency, are evaluated by the impedance-based stability criterion. The frequency range of effective impedance-based stability analysis is first identified. The effect of each inverter on the system harmonic instability is then identified by case studies on different groups of inverters. Lastly, the PSCAD/EMTDC simulations on a system with five passively-damped, LCL-filtered inverters are performed to verify theoretical analysis. It shows that the impedance-based stability analysis results agree with the time-domain simualtions provided that the frequency of concerns are around the half of the Nyquist sampling frequency.***

Keywords—Impedance-Based Stability Criterion; PSCAD; LCL-filter; Harmonic Stability; Paralleled Inverters

I. INTRODUCTION

In these days, many alternative energy resources have been developed to meet the expected future electric energy consumption and they are now widely commercialized [1]. However, as new energy resources are employed in the existing AC distribution network, unidentified crucial problems are being raised. In a Dutch distribution network with a high penetration of Photovoltaic (PV) generation, it has been showed that occasionally the PV inverters were switched off undesirably or exceeded the harmonic regulations [2]. Even though each of the PV inverter meets the grid codes, the power quality at the Point of Common Coupling (PCC) may still exceed the requirement [2], [3]. To address and mitigate these undesirable phenomena, the Impedance-Based Stability Criterion (IBSC) is emerging as an effective analysis tool [2]–[4]. The IBSC was originated from the design of input filters for DC-DC converters [5], which was later extended to study the dynamic interactions of the multiple interconnected dc-dc converters. Recently, the IBSC is applied to the AC distributed power systems with multiple inverters in [4], [6]. However, the IBSC is based on the small-signal models of inverters [7], which is only effective for the frequencies well below the switching frequency.

Unlike the existing low-frequency instability problems caused by the outer power control and grid synchronization loops, the harmonic instability, which are caused by the dynamic interactions of the fast inner current or voltage control loops of inverters, may exibit resonances in a wide frequency range. Moreover, these inner control loops may further interact with the output LCL-filters, resulting in a much higher frequency of oscillations [2], [3]. Hence, it is important to identify the effective frequency range of the IBSC for harmonic stability analysis.

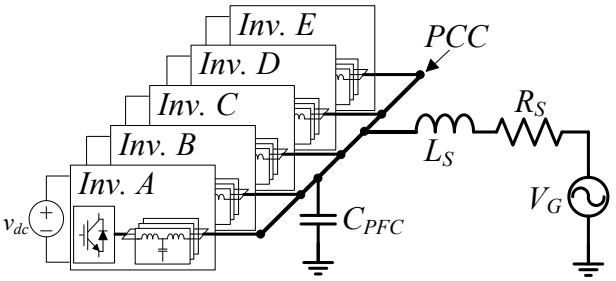

Fig. 1. Single line diagram of 3-phase distribution power system with five inverters in parallel.

This paper presents the harmonic stability assessment for a balanced three-phase system with five paralleled inverters, as shown in Fig. 1. The accuracy of the IBSC is evaluated for the high-frequency resonances. 1. All of the inverters are furnished with the passively damped LCL-filters and their power ratings are designed according to the Cigré LV benchmark system [8], [9]. To mimic the high-frequency conditions of the inverters and the grid in the average model, the resonance frequencies of the inverters are set around half of the Nyquist sampling frequency. The results are compared to time-domain simulation in order to check the modeling errors. Therefore, two different simulations for comparison are performed. One is looking for the effect of the grid impedance variation for a stable power system. The other one investigates possible unstable operating conditions among inverters. Finally, the IBSC can estimate the instabilities of the PE-based system which contains the inverter filter resonances which are about half of the Nyquist sampling frequency. Additionally, it is able to detect differences in the grid inductance variation as low as 10 *uH* for a given simulation condition and also to estimate some of the unstable cases accurately.

This work was supported by the European Research Council (ERC) under the European Union's Seventh Framework Program (FP/2007-2013)/ERC Grant Agreement no. [321149-Harmony].

II. System Description and Modeling

A. Distribution Power System with Inverters in Parallel

As shown in Fig. 1, the system contains five different ratings of three-phase Voltage Source Inverters (VSI) in parallel. All are connected to the PCC and are operated in grid connected mode, e.g. are able to inject active or reactive powers to the grid. For simplification, the connected distributed energy sources are assumed as constant DC voltage sources for all the inverters. There is a three-phase capacitor C_{PFC} connected to the PCC in parallel, which might be used for Power Factor Correction (PFC) for an existing load system like Direct-On-Line (DOL) startup motor application. The grid voltage is set as line to line rms 400 *V* at 50 *Hz*. The default value of the PFC capacitor is 12 *uF*. The grid impedance consists of a 400 *uH* inductance and a 0.1 *Ω* resistor, series connected.

B. Time-Domain Model for the Grid Inverter.

For the PSCAD/EMTDC time-domain simulation, the inverter model with the stationary axis Proportioal+Resonant (P+R) controller for the grid side current i_g is used as shown in Fig. 2 [10]. All inverters have the same filter structure which is the Inductor–Capacitor-Inductor (LCL) filter. The LCL filters are designed under the IEEE-519 [11] harmonic recommendation. Also, there are parasitic components such as the Equivalent Series Resistance (ESR) for each of the filter components. Further, the passive-damping resistor R_d is placed in series with capacitor C_f for stabilizing the inverter stand-alone. The inverter model uses the Sinusoidal Pulse Width Modulation (SPWM) method and sampling delay represented as an exponential delay function. Filter parameters, resonance frequencies of the inverters and controller gains are summarized in TABLE I.

C. Small Signal Model for the Grid Inverter

In order to use the IBSC for the analysis, the small signal models of the output admittance are used [4] and a grid inverter with current controller is modeled as shown in Fig. 3. The adopted current controller G_c is a P+R controller, while the time delay G_d which takes into account the digital implementation [12] and their transfer functions are as follows:

$$G_C = K_P + \frac{K_I s}{s^2 + w_0^2} \tag{1}$$

$$G_d = e^{-1.5T_s s} \tag{2}$$

where, the K_P and K_I are the controller proportional and integral terms, while w_0 is the grid frequency. T_s is the sampling time and the inverse of the switching frequency f_s.

]Y_M denotes the filter grid current to converter voltage transfer function, Y_O is the filter output admittance and Y_L is the control to output transfer function, respectively:

$$Y_M = \left.\frac{i_g}{v_M}\right|_{v_{PCC}=0} = \frac{Z_{Cf}}{Z_{Cf}Z_{Lf} + Z_{Lg}Z_{Lf} + Z_{Cf}Z_{Lg}} \tag{3}$$

$$Y_O = \left.\frac{-i_g}{v_{PCC}}\right|_{v_M=0} = \frac{Z_{Lf} + Z_{Cf}}{Z_{Cf}Z_{Lf} + Z_{Lg}Z_{Lf} + Z_{Cf}Z_{Lg}} \tag{4}$$

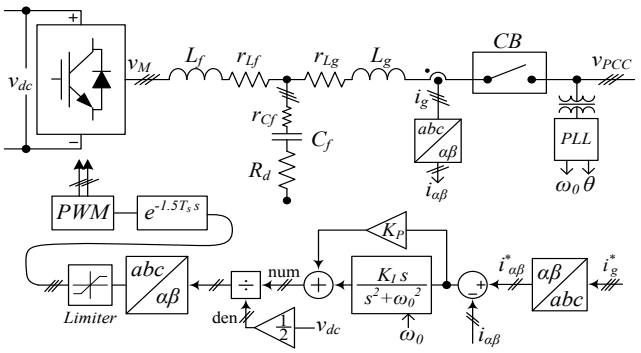

Fig. 2. Grid inverter control diagram for PSCAD implementation.

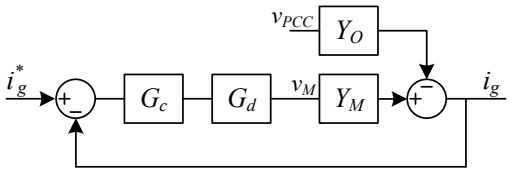

Fig. 3. Small signal representation of the grid inverter under 3-phase balanced load condition.

TABLE I. Grid Inverter specifications and parameters

		Inverter name				
		Inv. A	***Inv. B***	***Inv. C***	***Inv. D***	***Inv. E***
Power rating [kVA]		35	25	3	4	5.5
Base Frequency, f_0 [Hz]		50				
Switching Frequency, f_s [kHz] (Sampling Frequency)		10		16		10
DC-link voltage, v_{dc} [kV]		0.75				
Harmonic regulations of LCL filters		IEEE519-				
		1992	1992	1992	1992	2014[a]
Filter values	L_f[mH]	0.87	1.2	5.1	3.8	0.8
	C_f[uF]/R_d[Ω]	22/0.2	15/1.4	2/7	3/4.2	15/0.9
	L_g[mH]	0.22	0.3	1.7	1.3	0.2
Parasitics values	r_{Lf}[mΩ]	11.4	15.7	66.8	49.7	10
	r_{Cf}[mΩ]	7.5	11	21.5	14.5	11
	r_{Lg}[mΩ]	2.9	3.9	22.3	17	2.5
Controller gain	K_P	5.6	8.05	28.8	16.6	6.5
	K_I	1000	1000	1500	1500	1000
Resonance frequency [kHz]		2.55	2.46	3.01	2.87	3.05

[a] : new regulation, refer to [11]

where, the impedances Z_{Cf}, Z_{Lf} and Z_{Lg} are defined as follows :

$$Z_{Cf} = r_{Cf} + \frac{1}{sC_f} + R_d,\ Z_{Lf} = r_{Lf} + sL_f,\ Z_{Lg} = r_{Lg} + sL_g$$

The open loop gain T of the negative feedback loop shown in Fig. 3 is defined as follows:

$$T = G_C G_D Y_M \tag{5}$$

Finally, the closed loop control to output transfer function G_{CL} and the closed loop output admittance Y_{CL} can be obtained for each given modeling condition.

$$G_{CL} = \left.\frac{i_g}{i_g^*}\right|_{v_{PCC}=0} = \frac{T}{1+T} \tag{6}$$

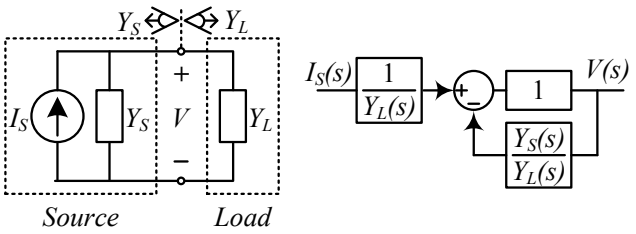

(a) (b)

Fig. 4. Small-signal admittance representation of: (a) an interconnected system with current source; (b) the minor loop gain representation.

$$Y_{CL} = \left.\frac{-i_g}{v_{PCC}}\right|_{i_g^*=0} = \frac{Y_O}{1+T} \tag{7}$$

D. Minor Loop Gain for the IBSC

The IBSC simplifies the complex impedance/admittance ratios of the power system into two equivalent values, namely the source admittance Y_S and the load admittance Y_L as shown in Fig. 4 (a). The Y_S is the object of the stability analysis and the Y_L is the sum of all admittances appeared on the terminal of Y_S. The minor loop gain T_M can be obtained from the two admittances as follows:

$$T_M = \frac{Y_S}{Y_L} \tag{8}$$

The stability of a given power system can be analyzed by using (8). It can be treated as an open loop transfer function of the closed loop system. The Nyquist stability criterion can be used for analyzing the stability of the system.

III. System Design and Simulation

A. Stand-alone Stable Inverter Design

One of the IBSC in prerequisites is that all analyzed inverters should be stable stand-alone. In order to obtain that, each of the inverter is designed to fulfill the Nyquist stability criterion as shown in Fig. 5. The loop gain T_X of the inverter X can be obtained systematically using (1)-(5), where the subscript $_X$ denotes the inverter name. The five inverters are stable individually, because there are no Right-Half-Plane (RHP) poles in the inverter loop gains and no encirclements in the Nyquist plots illustrated in Fig. 5. The considered parameter values are also summarized in TABLE I.

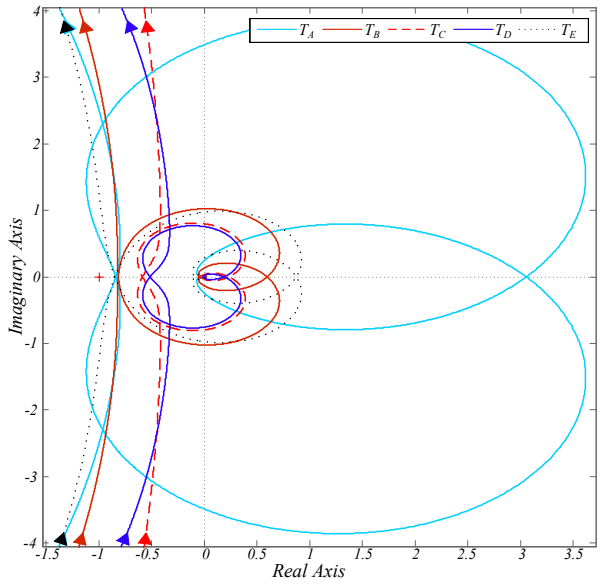

Fig. 5. Stand-alone stable inverters designed by the Nyquist plot

B. The Minor Loop Gain for the Accuracy Measurement

In order to measure the accuracy of the IBSC, the minor loop gain is modeled from Fig. 1. There are five inverters in parallel with a capacitor and a grid impedance. The accuracy is measured while varying the grid impedance. So, the object for the IBSC is the grid admittance Y_G which in this case can be seen as a source admittance Y_{SG}. The sum of the rest of the power system components becomes the load admittance Y_{LG}. Finally, the minor loop gain for the grid impedance T_{MG} is obtained as follows:

$$Y_{SG} = Y_G = \frac{1}{R_S + sL_S} \tag{9}$$

where, R_S is grid resistance and L_S is grid inductance as shown in Fig. 1.

$$\begin{aligned} Y_{LG} &= Y_{CPFC} + \sum_{X=A}^{E} Y_{CLX} \\ &= sC_{PFC} + Y_{CLA} + Y_{CLB} + Y_{CLC} + Y_{CLD} + Y_{CLE} \end{aligned} \tag{10}$$

where, Y_{CPFC} denotes the capacitor admittance of C_{PFC} as shown in Fig. 1.

$$T_{MG} = \frac{Y_{SG}}{Y_{LG}} \tag{11}$$

Before proceeding with the IBSC, another condition that should be satisfied is the stability of $1/Y_L$, which is depicted in Fig. 4 (b). To check the stability of $1/Y_L$ term, the pole zero

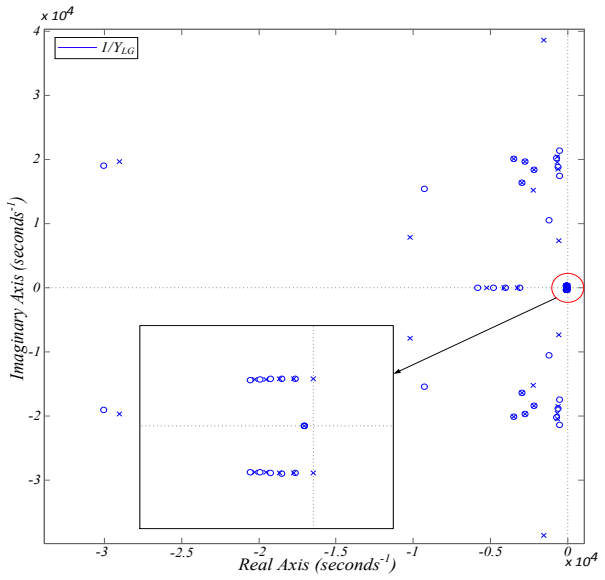

Fig. 6. Pole zero map of the inverse of the load admittance $1/Y_{LG}$

map method is used. In Fig. 6 it is shown that there are no RHP poles, hence the second prerequisite of the IBSC method is satisfied.

C. *Accuracy Measurement of the IBSC*

Accuracy of the IBSC can be measured by using the minor loop gain from (11). The grid inductance L_S is varied to change the source admittance Y_{SG} in (9) and the load admittance Y_{LG} in (10) is fixed during this variation. Each variation in Y_{SG} results in different minor loop gains T_{MG} which can further be compared with the time-domain simulation results.

Variations are made by varying L_S value from 100uH to 400uH and the trajectory is represented as red arrows with dotted lines as shown in Fig. 7. The two diagrams in Fig. 7 are not encircling the (-1, *j*0) point, hence the power system with both L_S cases is stable. However, there is a range of grid inductance values that makes the Nyquist plot of T_{MG} to encircle the (-1, *j*0) point, as shown in Fig. 8. The accuracy is measured by the value which moves the plot in the vicinity of the (-1, *j*0) point. The plot moves from the stable value (L_S = 155 *uH*) and passes the unstable values (L_S = 165 uH~260 *uH*) and becomes stable (L_S = 275 *uH*) again.

Time domain simulations are performed for all L_S values in Fig. 7 and Fig. 8. All the inverters are connected to the PCC and their output current references are set to be zero in order to see the effect of instability clearly. The parameter values for

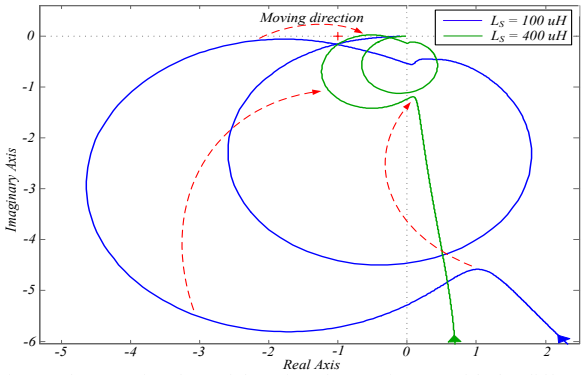

Fig. 7. The Nyquist plots of the minor loop gain T_{MG} with the different grid inductance L_S and its moving trajectory as L_S increases.

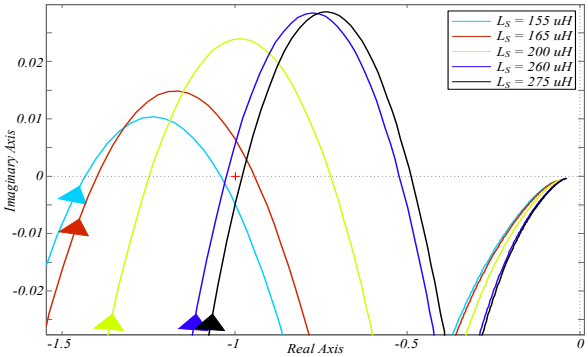

Fig. 8. The Nyquist plots for the marginally stable values of L_S.

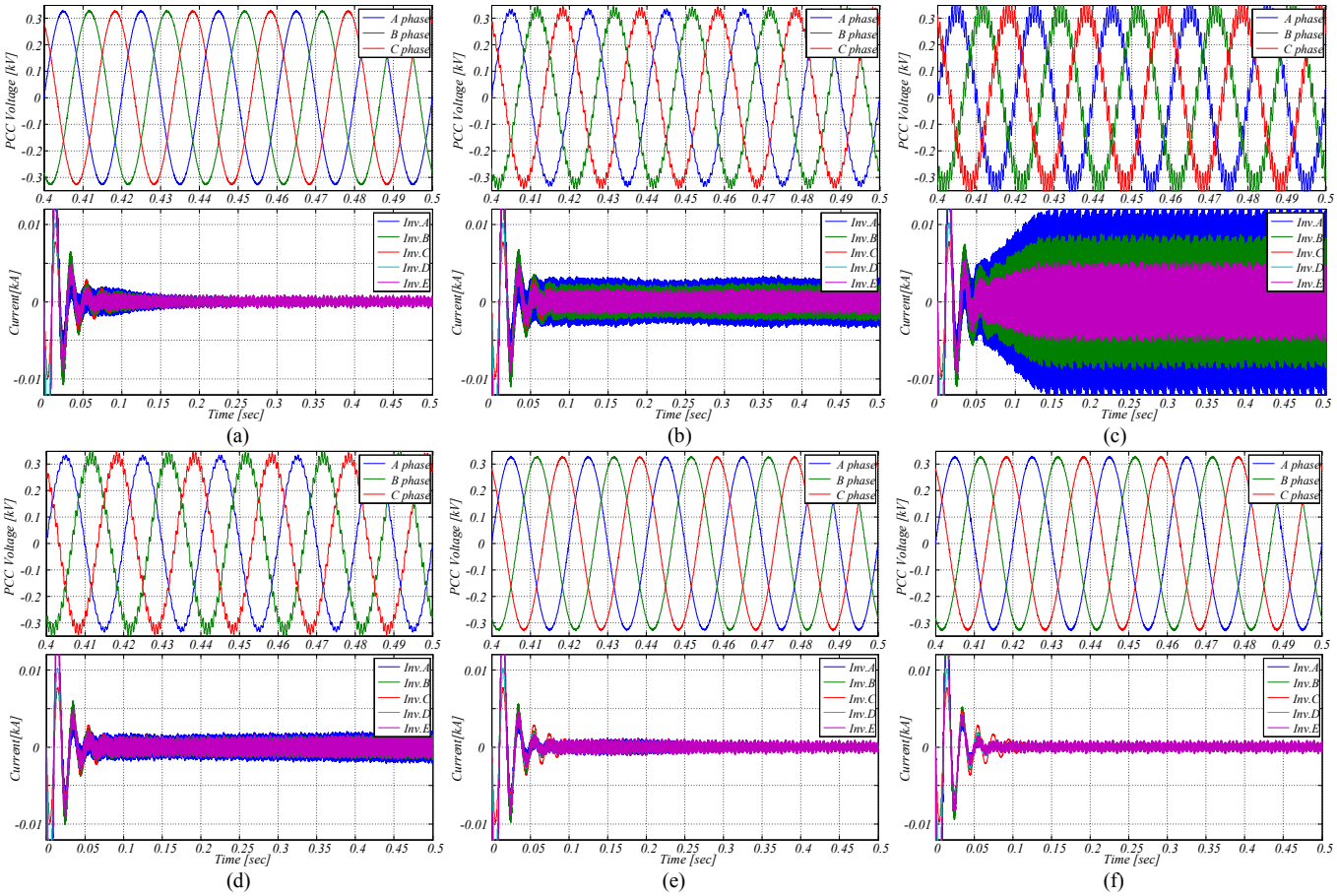

Fig. 9. Time-domain simulation of the test system in Fig.1 with the different values of L_S at no-load condition, PCC voltage (upper) and inverter currents (lower) : (a) 155uH; (b) 165uH; (c) 200uH; (d) 260uH; (e) 275uH; (f) 400uH.

the simulation are illustrated in Section II. In Fig. 9 are shown the PSCAD time-domain simulation results. It matches with the results in Fig. 7 and Fig. 8. At first, like in Fig. 7, when the Nyquist plot represents stable conditions, the voltage waveforms of the PCC does not contain distorted waveform and the output current of the inverter reaches steady state quickly as shown in Fig. 9 (f).

However, when the Nyquist plot moves in the vicinity of (-1, *j*0) point and does not encircle the point like 155 *uH* case in Fig. 8, it has a slightly longer time to reach the steady state current as shown in Fig. 9 (a) compared to the stable case in Fig. 9 (f). When it starts to encircle the (-1, *j*0) point it becomes unstable as shown in Fig. 9 (b). It becomes even worse when it approaches more to the unstable region, e.g. for 200 *uH* case in Fig. 8 which corresponds to Fig. 9 (c). Further, the Nyquist plot reaches another interception point like the 260 *uH* case. Oscillations in the PCC voltage and the inverter currents are much reduced. A more increment in the inductance value makes the system stable again as shown from 275 *uH* case until 400 *uH* .

D. Unstable Combinations of the Inverters

The previous section deals with the unstable condition caused by the grid impedance variation. However, unlike the previous section, the unstable conditions may also occur by the inverter presence in the power system. When one or more inverters operate in the power system, the load admittance Y_L is changed and the stability of the power system is affected. In order to give an example of such stability variations, a stable system with L_S = 400 *uH*, as shown in Fig. 7, is selected as reference. For this case, the inv. A is selected as the source admittance Y_{SA} as presented in (12). The load admittance in (13) which is seen from the inv. A includes the equivalent

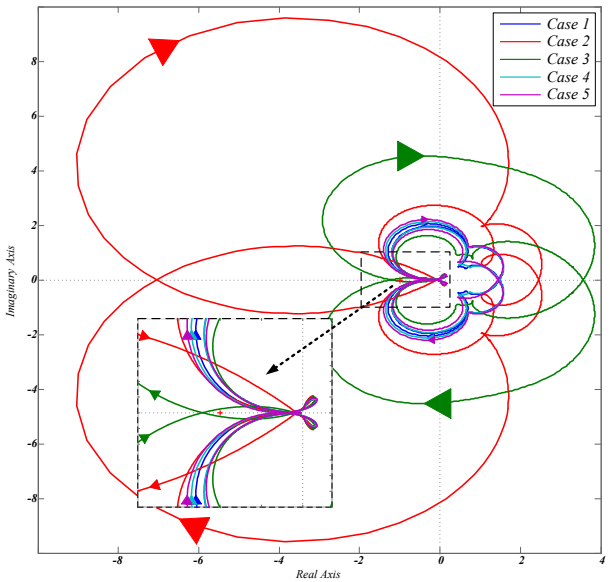

Fig. 10. The Nyquist plot of the minor loop gain T_{MA} for different cases of the load admittances Y_{LA}.

admittances of all the other inverters in the power system and the grid admittance. In (14)-(17) some of the inverters are consequently eliminated from Y_{LA} in order to illustrate different operating scenarios, e.g. disconnection of some inverters in the power system. The unstable case at PCC can be found by analyzing the minor loop gain T_{MA} from (18) derived for the load admittances expressed in (13)-(17). Fig. 10 shows the estimated stability analysis results from the different minor loop gains.

$$Y_{SA} = Y_{CLA} \tag{12}$$

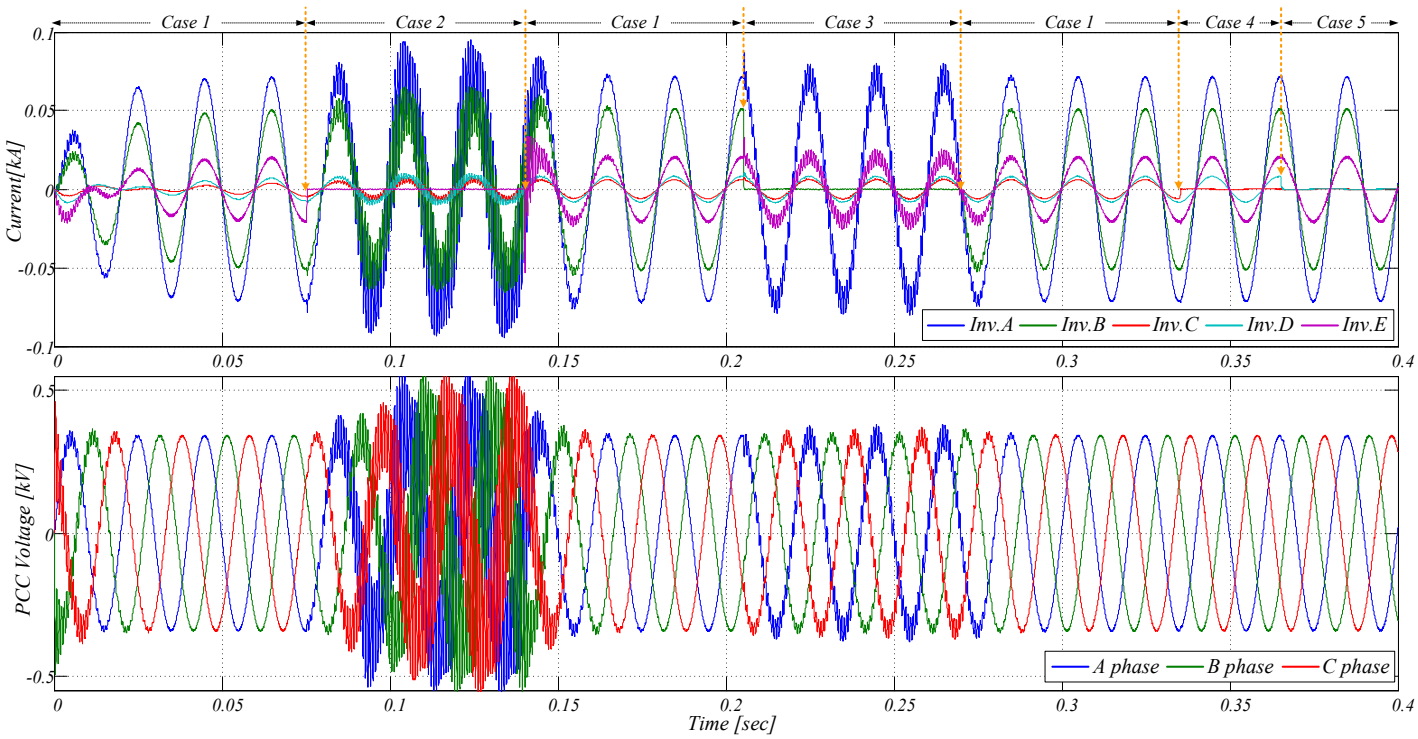

Fig. 11. Time-domain simulation for all cases in Fig. 10 with full load inverter condition : the inverter phase currents (upper) and the PCC voltage (lower).

$$Case\,1: Y_{LA} = Y_G + Y_{CPFC} + Y_{CLB} + Y_{CLC} + Y_{CLD} + Y_{CLE} \quad (13)$$

$$Case\,2: Y_{LA} = Y_G + Y_{CPFC} + Y_{CLB} + Y_{CLC} + Y_{CLD} \quad (14)$$

$$Case\,3: Y_{LA} = Y_G + Y_{CPFC} + Y_{CLC} + Y_{CLD} + Y_{CLE} \quad (15)$$

$$Case\,4: Y_{LA} = Y_G + Y_{CPFC} + Y_{CLB} + Y_{CLD} + Y_{CLE} \quad (16)$$

$$Case\,5: Y_{LA} = Y_G + Y_{CPFC} + Y_{CLB} + Y_{CLE} \quad (17)$$

$$T_{MA} = \frac{Y_{SA}}{Y_{LA}} \quad (18)$$

There are two unstable cases which encircle the (-1, *j*0) point, which are Case 2 and Case 3. As interpreted in the previous section, the Case 2 is more unstable than Case 3, because the minor loop gain is placed far from the (-1, *j*0) point.

In order to verify the estimated analysis results in Fig. 10, the time domain analysis is performed. In this time domain-simulation the current references are set to their rated currents. All cases are adjusted by turning on and off the Circuit Breaker (*CBs*) included in each inverter as depicted in Fig. 2. Fig. 11 reflects the exact analysis results obtained from the Nyquist plots in Fig. 10. In Case 1 the system is stable, when all five inverters are connected. However, when inv. B or inv. E is disconnected, the all power system becomes unstable as presented in Case 2 and 3. The disconnection of the inv. C and inv. D from the power system does not affect the system stability, which corresponds to Case 4 and Case 5. The presented scenarios illustrate some of the unstable/stable combinations of the power system components. The instabilities are caused by interactions among the controllers in each inverter.

IV. CONCLUSION

Two comparisons are performed to check the feasibility of the IBSC of PE-based power system with high resonance frequencies around the half of the Nyquist sampling frequency of the devices. It shows the IBSC results are very well matched with the time-domain simulation results and even it can detect the instability of 10uH deviation in the grid inductance for a given test condition. In addition, it is able to find out possible unstable cases caused by arbitrary connection of the inverters to the power system.

REFERENCES

[1] F. Blaabjerg, Z. Chen, and S. B. Kjaer, "Power Electronics as Efficient Interface in Dispersed Power Generation Systems," *IEEE Trans. Power Electron.*, vol. 19, no. 5, pp. 1184–1194, Sep. 2004.

[2] X. Wang, F. Blaabjerg, M. Liserre, Z. Chen, J. He, and Y. Li, "An Active Damper for Stabilizing Power-Electronics-Based AC Systems," *IEEE Trans. Power Electron.*, vol. 29, no. 7, pp. 3318–3329, Jul. 2014.

[3] X. Wang, F. Blaabjerg, and W. Wu, "Modeling and Analysis of Harmonic Stability in an AC Power-Electronics-Based Power System," *IEEE Trans. Power Electron.*, vol. PP, no. 99, pp. 1–1, 2014.

[4] J. Sun, "Impedance-Based Stability Criterion for Grid-Connected Inverters," *IEEE Trans. Power Electron.*, vol. 26, no. 11, pp. 3075–3078, Nov. 2011.

[5] R. D. Middlebrook, "Input filter considerations in design and application of switching regulators," *IEEE Ind. Appl. Soc.Annu. Meet.*, pp. 91–107, 1976.

[6] J. Sun, "Small-Signal Methods for AC Distributed Power Systems–A Review," *IEEE Trans. Power Electron.*, vol. 24, no. 11, pp. 2545–2554, Nov. 2009.

[7] R. W. Erickson and D. Maksimović, *Fundamentals of Power Electronics*. Boston, MA: Springer US, 2001.

[8] "Benchmark Systems for Network Integration of Renewable and Distributed Energy Resources C06.04.02," CIGRE, 2014.

[9] R. Beres, X. Wang, F. Blaabjerg, C. L. Bak, and M. Liserre, "A review of passive filters for grid-connected voltage source converters," in *2014 IEEE Appl. Power Electr. Conf. and Expo. - APEC 2014*, 2014, pp. 2208–2215.

[10] R. Teodorescu, F. Blaabjerg, M. Liserre, and P. C. Loh, "Proportional-resonant controllers and filters for grid-connected voltage-source converters," *IEE Proc. - Electr. Power Appl.*, vol. 153, no. 5, p. 750, Sep. 2006.

[11] "IEEE Recommended Practice and Requirements for Harmonic Control in Electric Power Systems," 2014.

[12] V. Blasko and V. Kaura, "A new mathematical model and control of a three-phase AC-DC voltage source converter," *IEEE Trans. Power Electron.*, vol. 12, no. 1, pp. 116–123, 1997.